TEMPERATURE DEPENDENCE OF A NiTi SHAPE MEMORY ALLOY'S SUPERELASTIC BEHAVIOR AT A HIGH STRAIN RATE

Weinong Chen and Bo Song

TEMPERATURE DEPENDENCE OF A NiTi SHAPE MEMORY ALLOY'S SUPERELASTIC BEHAVIOR AT A HIGH STRAIN RATE

WEINONG CHEN AND BO SONG

The temperature dependence of the dynamic compressive stress-strain behavior of a NiTi shape memory alloy (SMA) has been determined at a strain rate of 4.35×10^2 s^{-1} with a split Hopkinson pressure bar (SHPB) modified for obtaining the dynamic stress-strain loops at constant strain rates. The environmental temperature was varied from 0 to 50° C, where the SMA exhibits superelastic behavior through stress-induced martensite (SIM). Experimental results show that both the loading and unloading portions of the stress-strain loop are significantly temperature dependent. Shape memory effect below the austenite finish transition temperature, A_f, and superelastic behavior above A_f are also observed at the high strain rate.

1. Introduction

Engineering and medical applications of shape memory alloys (SMA) have attracted research efforts to reveal the mechanical responses of these materials. Recent research in the field is extensively reviewed, for example, by [Birman 1997], [Otsuka and Wayman 1988], [James and Hane 2000], and [Bhattacharya and James 2005]. Reversible martensitic phase transformations provide SMA's with the capabilities of shape memory and superelastic deformation. An SMA possesses an austenite phase at high temperature and a martensitic phase at low temperature. There is a range of transition temperatures over which temperature-induced phase transformation occurs. An object that appears to be permanently deformed at low temperature in its martensitic phase will return to its original shape in austenite phase when heated above the transition temperature, because of a solid phase transformation from martensitic back to austenite. Two-way shape memory has also been proposed where the alloy remembers its shapes at both low and high temperatures [Wayman 1993]. It has been proposed that the shape memory effects may be utilized to build small-scale machines [Bhattacharya and James 2005].

In addition to the temperature-induced phase transformations, martensitic transformation can be induced by mechanical stress in a certain temperature range. The

range starts just above the temperature-induced phase transformation region (typically marked by the austenite finish transformation temperature A_f) and ends at a temperature above which stress-induced martensitic transformation is no longer possible, M_d [Stoeckel and Yu 1991; Wayman 1993; Duerig and Pelton 1994]. The alloy is austenite in this temperature range when stress-free. When the applied stress exceeds a threshold level, called the on-set stress for stress-induced martensite (SIM), the austenite crystal structure will transform into a martensitic phase. Therefore, martensitic transformation in the material can occur at much higher temperatures when assisted by mechanical stress. This SIM-induced deformation is achieved by detwinning [Bhattacharya 2003; Liu et al. 2002], which requires much less energy than to deform the austenite by conventional metal deformation mechanisms. It takes a stress level an order of magnitude higher to deform the austenite material than the martensite at the same strain [Wayman 1993]. The detwinning in the martensitic phase can accumulate up to 10% strain, which can be recovered completely by the reverse transformations back to austenite when the applied stress is removed. This large but reversible deformation is named superelasticity, a distinct property of SMA's.

When the temperature is in the superelasticity range, $A_f < T < M_d$, the typical stress-strain curve of an SMA obtained under quasistatic loading conditions at engineering strain rate, $\dot{\varepsilon} = 1.2 \times 10^{-4}$/s is shown in Figure 1 [Song and Chen 2004].
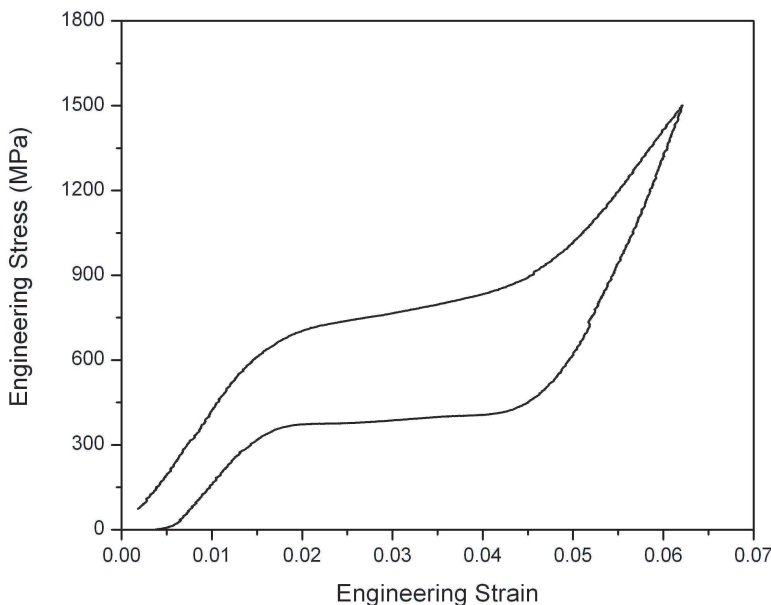
Figure 1. A quasistatic stress-strain curve of a NiTi SMA.

The compressive stress-strain curve contains two plateaus. The upper plateau corresponds to the loading portion where mechanical stress drives the austenite to transform into martensite and where detwinning occurs in the newly formed SIM. The lower plateau represents the stress-strain behavior of the SMA during the unloading process where the SIM is transforming back to austenite. Thermal energy is needed to assist this reverse transformation. This stress-strain curve indicates that, even though the mechanical behavior is termed superelastic because there is hardly any permanent deformation upon unloading, part of the mechanical energy used to deform the alloy is lost during unloading. Therefore, the loading/unloading cycle on the SMA leaves no permanent deformation, but dissipates mechanical energy. The volume density of the lost energy in a loading/unloading cycle can be computed from the area within the hysteresis loop on the stress-strain curve shown in Figure 1. Such an energy loss over a loading/unloading cycle makes it possible for the shape memory alloy to be used as a shock/vibration absorption medium. In fact, SMA's have been described as "quiet" alloys [Schetky and Perkins 1978]. In order to properly use the SMA's as an energy-absorbing member in applications subjected to high-rate loading, it is essential to quantitatively determine and understand the constitutive behavior of these alloys under dynamic loading conditions.

Considerable research efforts have been focused on the dynamic mechanical responses of SMA's under high rates of loading. Ogawa [1988] used a conventional split Hopkinson pressure bar (SHPB) and characterized a shape memory alloy over a temperature range of 201 K to 363 K. Lin et al. [1996] and Wayman [1993] studied the rate effects on the mechanical behavior of a NiTi alloy within the quasistatic range. Chen et al. [2001] determined the compressive behavior of a NiTi SMA over the strain rate range of 0.001–750 s^{-1}. A modified SHPB was used to control the loading profile such that the loading portion of the stress-strain curve was obtained at a constant strain rate. It was found that the on-set stress for SIM depends on the strain rate, and that the strain history in the specimen lags behind the stress history. Similar high-rate experimental results have also been reported recently in compression by Nemat-Nasser et al. [2005] and Nakayama et al. [2005], and in tension by Liu et al. [2002]. By using a smaller specimen to achieve higher strain rates in their dynamic compression experiments, Nemat-Nasser et al. [2005] found that the stress-strain relation of their NiTi SMA differs from that achieved at a moderately high strain rate. By comparing the shape memory effects produced by different rates of loading, Belyaev et al. [2002] discovered that an increase in strain rate can lead to an increase in shape memory effect. At even higher strain rates, Millett et al. [2002] studied the shock response of NiTi SMA. Dai et al. [2004] investigated the propagation of macroscopic phase boundaries under impact loading analytically and numerically, and found that the thermal effect should be taken into account due to the temperature coupling nature of the phase transition process. The effects of

loading conditions other than one-dimensional were explored recently [McNaney et al. 2003]. Besides the experimental research, analytical modeling is also under intensive development; examples include [Lagoudas et al. 2003], [Iadicola and Shaw 2004], and [Lovey et al. 2004].

Although the mechanical behavior of SMA's has been experimentally explored recently at high strain rates, most dynamic experiments have been performed in a controlled manner only during the loading portions of the stress-strain curves. The unloading portions have been left uncontrolled due to difficulties in dynamic experimentation. However, since both of the loading and unloading portions of stress-strain curves for an SMA are important in determining the energy absorbing capacity of the material at high rates, it is desirable that the loading conditions during both loading and unloading stages in a dynamic experiment be precisely controlled to produce dynamic loading and unloading stress-strain loops at constant strain rates. Furthermore, most of the dynamic experiments are performed at room temperature. Since the superelastic behavior of SMA's only exists within a certain temperature range, it is important to determine the high-rate behavior over this temperature range. In this paper, we employ a recently developed SHPB technique, which produces dynamic compression experimental results for a stress-strain loop at a common constant strain rate over both loading and unloading portions [Song and Chen 2004], to conduct the dynamic compressive experiments on a NiTi SMA at a high strain rate over a temperature range where superelastic behavior is clearly observed.

A valid SHPB experiment requires that the specimen undergo homogeneous deformation under dynamic stress equilibrium [Gray 2000; Song et al. 2003]. In addition, a constant strain rate is convenient for the purpose of developing more accurate constitutive models based on experimental results. To ensure that these conditions were satisfied when dynamically testing the SMA specimens using a SHPB in this study, pulse shaping techniques were employed to control both the loading and unloading portions of the incident pulse so that the specimen was deformed under valid dynamic testing conditions. The dynamic stress equilibrium in the specimen was monitored using 1-wave/2-wave analysis [Gray 2000] on the nearly nondispersive waves created by the pulse-shaping technique. Experiments were conducted on Nitinol SE508 SMA. The following sections briefly describe the experiments and then present the results for the NiTi alloy.

2. Experimental setup and specimen preparation

2.1. *Experimental setup of the modified SHPB.* To study the dynamic compressive loading/unloading behavior of the SMA, a SHPB with pulse shaping on both loading and unloading stages [Song and Chen 2004] was used to conduct dynamic
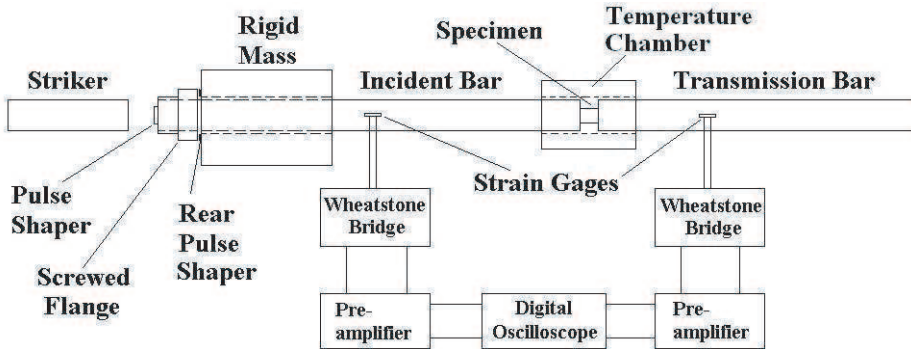
**Figure 2.** A schematic of the modified split Hopkinson pressure bar.

compressive experiments. A temperature chamber covered the testing section of
the SHPB. A schematic of the modified SHPB facility is shown in Figure 2. In
addition to the striker, incident and transmission bars included in a standard SHPB,
the modified SHPB apparatus consists of front and rear pulse shapers in association
with a momentum trapping system to facilitate constant strain-rate loading and
unloading on the specimen. The front pulse-shaper is attached at the impact end of
the incident bar to control the loading profile in the incident pulse; the rear pulse-
shapers are placed on the surface of the rigid mass. A gap between the flange,
which is screwed on the impact end of the incident bar, and the rigid mass, through
which the incident bar passes, is precisely preset. Upon the impact of the striker
during an experiment, the front pulse shaper is extensively compressed, generating
a desired incident loading profile to deform the specimen at a constant strain rate
under dynamic stress equilibrium over the loading phase of the experiment. In
the meantime, a compression wave is also generated and then propagates in the
striker. This compression wave is reflected back as an unloading wave (tension
wave) when it arrives at the free end of the striker. The unloading pulse from the
striker travels into and then passes through the incident bar to unload the specimen.
In this momentum trap design, the gap between the flange and the rigid mass is
precisely controlled to close before the unloading pulse travels into the incident
bar. The rear pulse shapers on the surface of the rigid mass are compressed by the
flange, generating a desired unloading profile in the incident bar. The unloading
pulse is well designed by varying the dimensions of the rear pulse shapers to ensure
that the specimen recovers at the same constant strain rate under dynamic stress
equilibrium during unloading. Thus, a dynamic stress-strain loop is obtained at the
same constant loading and unloading strain rate.

In the modified SHPB, a heating/cooling chamber is placed between the incident bar and the transmission bar (around the specimen) to create environmental temperatures that are monitored with an embedded thermocouple inside the heater/cooler chamber. Heating is automatically controlled by a temperature controller, manufactured by WATLOW (96A0-DAAA-00RG), while cooling is manually controlled by pouring liquid nitrogen into a surrounded 6.0 mm diameter brass tube inside the heater/cooler. The environmental temperature inside the chamber is controlled through the flow rate control of liquid nitrogen inside the brass tube when testing below room temperature. This temperature chamber was used in SHPB experiments on other materials and its details were described in a previous paper [Song et al. 2005]. Furthermore, besides the environmental temperature, the adiabatic temperature rising and falling during the forward and reverse SIM in the specimen is monitored by a small thermocouple embedded in one of the specimens. The specimen temperature measuring technique was also previously employed and a detailed description of it can be found in a previous publication [Song et al. 2003].

The lengths of the VascoMax maraging steel bars used for the experiments were 1830, 762, and 305 mm for the incident, transmission, and striker bars, respectively, with a common diameter of 12.3 mm. The strain signals sensed by strain gages from the incident and transmission bar surfaces were recorded using a high-speed digital storage oscilloscope. Since the temperature variation range (0–50° C) in the chamber is not significant enough to affect the stress-wave propagation through the temperature gradient along the bar length, the temperature gradient effects on the wave propagation in the bars are neglected in data reduction.

2.2. *Materials and specimens.* The SMA investigated in this research is NDC (Nitinol Devices & Components, Fremont, CA) SE508, nominally 55.8% nickel by weight and the balance titanium. The specified density is 6.5 g/cm^3, with an austenite finish transition temperature A_f of 5–18° C and a melting point of 1310° C, as provided by the manufacturer. The temperature above which stress-induced martensitic transformation is no longer possible, M_d, for SE508 is approximately 150° C. The temperature range for this alloy to exhibit superelasticity (the capability of returning to its original shape upon unloading after a substantial deformation) is 15–150° C. In a previous study [Chen et al. 2001], it was found that the strain far lagged behind the stress during the dynamic unloading stages in experiments performed at room temperature (close to A_f), indicating that there may exist unique dynamic deformation phenomena in the alloy during high-rate unloading near room temperature. However, the unloading paths were uncontrolled in those experiments. Therefore, the choice of the temperature range in this study reflects the effort to focus on the behavior near A_f (0–50° C) under much better controlled experimental conditions.
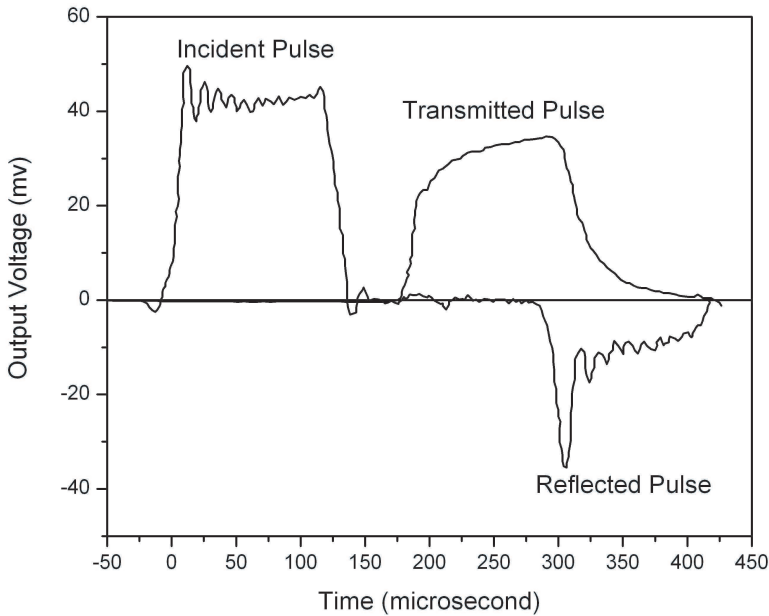
Figure 3. Typical oscilloscope records of a conventional SHPB experiment on an SMA.

Cylindrical specimens of 5.94 mm diameter by 6.10 mm long were sliced from a heat-treated Nitinol rod with a water-jet cooled abrasive saw. Chilled water was continuously sprayed on the contact area of the cutting blade and the Nitinol bar to keep the temperature low in the NiTi alloy during machining.

2.3. *Dynamic experimental technique for the SMA.* When the SHPB is used in its conventional configuration, there are high-frequency oscillations riding on the base incident pulse as shown in Figure 3. These oscillations in the loading pulse profile, which are the results of wave dispersion due to radial inertia effects when the wave propagates in the bars, cause complications in the loading conditions in the specimen. The nature of stress-induced phase transformation makes the specimen sensitive to alternations of loading and unloading. Figure 3 shows a typical oscilloscope record of an SMA undergoing dynamic loading by a conventional SHPB. There is no plateau in the reflected pulse shown in Figure 3, which indicates that the specimen does not deform at a constant strain rate. The oscillations in the reflected pulse also indicate that the specimen experiences a complicated deformation process. The point-wise dynamic material properties extracted by averaging the response over the specimen's volume cannot be expected to be accurate and reliable when the specimen is undergoing such a complicated deformation.

In order to obtain reliable dynamic material behavior from an SHPB experiment
for the SMA, the rapid oscillations in the incident pulse must be avoided. Further-
more, efforts must be made to ensure that a dynamic equilibrium stress state is
reached in the specimen during the experiment and to maintain a constant strain
rate in the specimen. A homogeneously-deforming specimen under a dynamic
equilibrium state of stress makes the volume-average of the specimen's behavior
representative of the point-wise material properties. A constant strain rate during
an experiment makes it convenient to report the stress-strain response as a function
of strain rates, which is necessary to fit material constants in constitutive models.
To obtain the stress-strain loop of an SMA at a constant strain rate, it is also de-
sirable to maintain the same strain rate during both loading and unloading phases
of the experiment. These requirements pose significant challenges in the dynamic
experiment design.

To eliminate the oscillations in the loading pulse and to ensure that the specimen
deforms at a constant strain rate in dynamic equilibrium, a pulse shaper was placed
on the impact end of the incident bar to control the shape of the loading pulse
(Figure 2). There are a variety of pulse-shaping devices. For example, Duffy
et al. [1971] used a pulse-shaper in the form of a concentric tube to smooth pulses
generated by explosive loading in a torsional Hopkinson bar. Ravichandran and
Chen [1991] and Frew et al. [2002] used copper pulse shapers to achieve ramp
loading profiles when testing ceramics and rocks using SHPB. Togami et al. [1996]
used a pulse shaper in a modified SHPB to control the loading pulse shape and
to filter out high-frequency components in the incident pulse for accelerometer
calibrations up to 200,000 g. In the present research, annealed C11000 copper
disks were used to control the shape of the loading pulse during both loading and
unloading phases. The diameters and the thickness of the pulse shapers necessary
to control the strain rate in the SMA specimen at a desired and constant level
were difficult to determine since the dynamic behavior of the SMA was unknown
before the experiments. Trial experiments were conducted to select a proper pulse
shaper for each combination of desired strain rate, environmental temperature, and
maximum strain.

3. Experiments and Results

3.1. *Dynamic experiments with the modified SHPB.* A typical set of incident,
reflected, and transmitted signals recorded with the oscilloscope for an SHPB
experiment on the NiTi SMA at 23° C with shaped pulses is shown in Figure 4.
The dashed line is the transmitted pulse, which records the stress history in the
specimen. The first pulse in the solid line is the incident pulse, whereas the second
and third are the reflected pulses associated with the deformations during loading
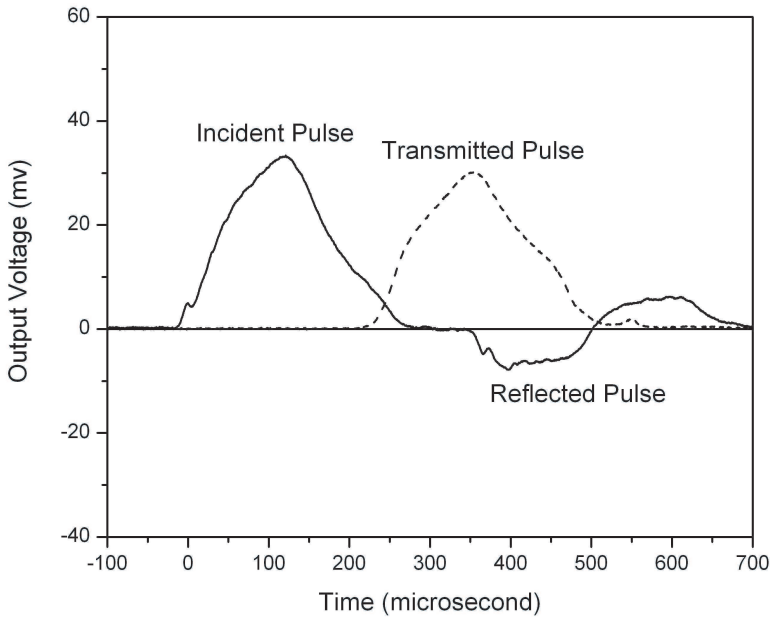
Figure 4. Oscilloscope records of a pulse-shaping SHPB experiment on a NiTi SMA.

and unloading in the specimen. If the specimen's mechanical impedance ($\rho c A$, where ρ is the mass density, c the bar wave velocity, and A the cross-sectional area) is less than that of the bar, the incident and first reflected pulses are opposite in sign, as seen in Figure 4. Furthermore, the second reflected pulse indicates the strain rate of the recovery deformation in the specimen and has an opposite sign from the first reflected pulse. Although the first and second reflected pulses have opposite signs, the magnitudes are nearly the same, which indicates that the strain rates at both the loading and unloading stages are nearly the same. We also note that the magnitudes of the reflected pulses are nearly constant in each of the reflected pulses, which indicates that the loading and unloading strain rates are nearly the same constant. This is a necessary condition to obtain a dynamic stress-strain loop or hysteretic loop at a certain strain rate. A comparison between the incident and reflected pulses of Figures 3 and 4 indicates that the shape of the incident pulse in the pulse-shaped experiment shown in Figure 4 is very different from that obtained in a conventional SHPB experiment (Figure 3). The high-frequency oscillations on the incident pulse shown in Figure 3 are eliminated after pulse shaping, as shown in Figure 4. The nearly flat and equal plateaus on the first and second reflected pulses shown in Figure 4 indicate that the specimen deformed at a nearly constant strain rate during both loading and unloading on the NiTi SMA specimen in a pulse-shaped SHPB experiment. The transmitted pulses were used to calculate stress
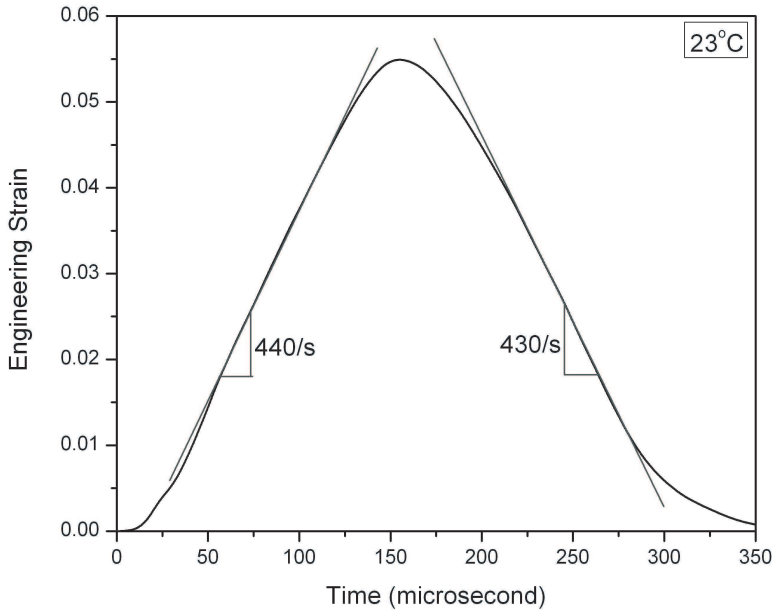
Figure 5. Dynamic loading and unloading strain histories in the NiTi Specimen.

history in the NiTi specimen according to conventional SHPB theory based on 1-D wave propagation theory [Kolsky 1949; Lindholm 1964; Follansbee 1985; Gray 2000]. The strain rate in the experiment was determined by the average magnitude of the plateau in the reflected pulses.

The dynamic strain history in the specimen is shown in Figure 5. An examination of Figure 5 shows that both the loading (rising) and unloading (descending) portions of the strain histories are nearly straight lines, indicating constant rates of deformation. The slope of the loading portion, that is, the loading strain rate, is observed to be 440/s, whereas that for the unloading portion is 430/s. Therefore, the strain rates during both loading and unloading stages may be considered as the same constant. It should be noted that the dynamic strain history in a NiTi SMA lags behind the dynamic stress [Chen et al. 2001; Song and Chen 2004], which needs to be taken into account in the pulse shaper design.

In SHPB experiments, dynamic stress equilibrium in the specimen is a fundamental requirement for valid data processing because equilibrium is one of the basic assumptions upon which SHPB theory is built [Meyers 1994; Gray 2000]. When dynamic equilibrium is impossible to reach, the constitutive behavior may be still found using a hybrid approach assisted by computer simulation if the form of the stress-strain relation is known. However, in the case of the NiTi SMA, the dynamic stress-strain relations need to be determined by the SHPB experiments.
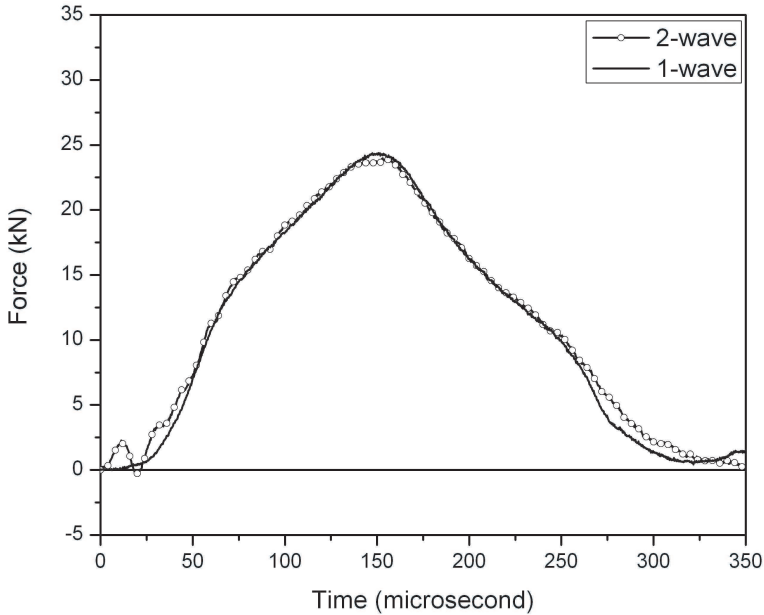
Figure 6. Dynamic equilibrium analysis by 1-wave/2-wave method.

Dynamic equilibrium must be achieved such that the volume average of the stress-strain behavior over the entire specimen may be used as the point-wise material responses at a certain strain rate. It is therefore critical to ensure that the dynamic equilibrium conditions are satisfied in order to obtain valid experimental results.

In our experiments, we checked stress equilibrium by comparing the transmitted signal (1-wave) with the difference between the incident and reflected signals (2-wave) [Gray et al. 1997; Wu and Gorham 1997; Gray 2000]. The incident waves created in our experiments by pulse shaping are nearly nondispersive since there are few high-frequency components associated with the main loading pulses. The results on stress equilibrium from 1-wave, 2-wave analysis are thus considered to be reliable. Figure 6 shows the results of such an analysis on the stress pulses of Figure 4. There are two nearly overlapping curves shown in Figure 6. One is the transmitted pulse profile (1-wave), and the other is the difference between the incident and the reflected pulses (2-wave). The 2-wave curve represents the axial force history on the face of the specimen that is in contact with the incident bar [Gray et al. 1997; Wu and Gorham 1997]. The 1-wave curve, which is used to calculate the stress history in SHPB data reduction, is the axial force history on the face of the SMA specimen that is in contact with the transmission bar during an experiment. Dynamic stress equilibrium in the specimen requires that the 1-wave and the 2-wave are the same over the duration of the SHPB experiment. Figure 6
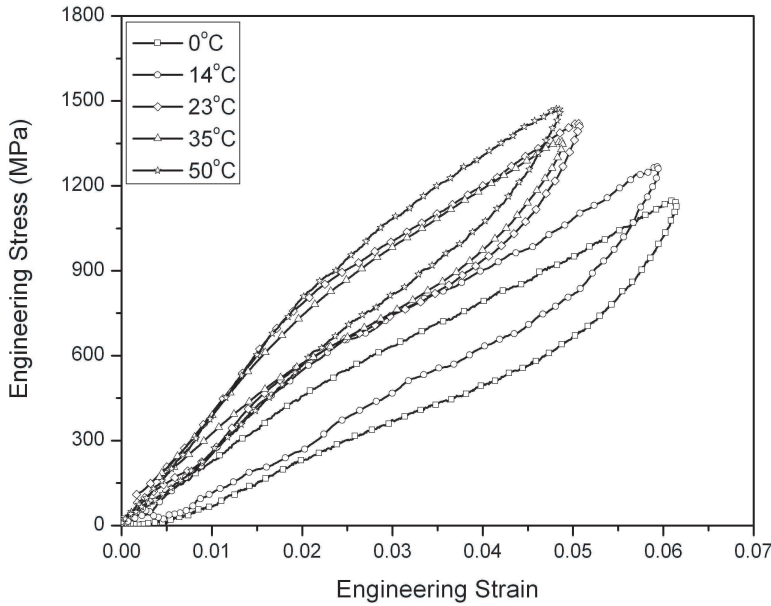
Figure 7. Dynamic compressive stress-strain curves of the NiTi SMA.

shows that the 1-wave curve nearly overlaps the 2-wave curve in this pulse-shaped experiment, which indicates that dynamic equilibrium stress state in the specimen has been achieved. It is noted that the fluctuations are observed in the 2-wave curve in Figure 6 within the first 20 μs. The slight wave dispersion, even though the pulse shaping technique was employed, may result in fluctuations in the subtraction of the reflected pulse from the incident pulse. However, the fluctuations do not affect the examination of the stress equilibration process in the specimen, as shown in Figure 6. The amplitude of the reflected pulses is nearly constant as shown in Figure 5, which indicates a constant strain rate over the duration of the experiment, including both loading and unloading phases. Therefore the SHPB experiment recorded in Figure 4 is a valid dynamic experiment. Such analysis was performed on every experiment presented in this paper.

3.2. *Dynamic stress-strain loops at various temperatures for the SMA.* Figure 7 summarizes the dynamic compressive stress-strain curves at a common dynamic compression strain rate of 430/s for the Nitinol SE508 SMA at environmental temperatures of 0°, 14°, 23°, 35°, and 50°. The stress-strain curves are plotted in the units of engineering stress and strain, which are nearly identical to true stress and strain curves, since the maximum strain ($\sim$ 6%) experienced by the specimens is small. As shown in Figure 7, the shape of the dynamic stress-strain curves has similarities and differences as compared to those obtained under quasistatic

loading conditions. The quasistatic compressive stress-strain curve obtained at a temperature well above A_f is typically in the form presented in Figure 1 (23° in this case). After a linearly elastic region, the stress-strain curve bends into a plateau-like region caused by stress induced martensite starting at a strain of $\sim$ 1.5–2%. If the deformation is too large (for example, > 4.5% strain), significant work-hardening in this SMA drives a steep rise in the stress-strain curve. The reverse transformation from martensite to austenite upon unloading takes place at a smaller stress, which is schematically displayed by the lower plateau in the stress-strain loop. At the dynamic strain rate of 430/s, we can examine one of the stress-strain curves (for example, at 23°) to illustrate its similarities and differences from its quasistatic behavior. Similar to the quasistatic case, the dynamic stress-strain curve also exhibits a linear initial portion up to a strain of $\sim$ 1.7–2%, where a transition in the stress-strain curve occurs (on-set stress for SIM). However, instead of following a plateau-like stress-induced martensite transformation region, the dynamic stress-strain curve displays a work-hardening behavior after the SIM on-set stress. A similar behavior is observed on the unloading branch of the stress-strain loop. There is no plateau observed for the reverse phase transformation. Instead, a delayed unloading curve that is nearly parallel to the loading curve is observed. This clear difference from quasistatic behavior may be an indication that SIM phenomena are rate dependent. Adiabatic temperature change in the specimen under high-rate deformation is considered to be one of the parameters that depicts this shape change in stress-strain curve from quasistatic to dynamic loading conditions. The discussion on this point will be continued after results on the adiabatic temperature change are presented.

The results shown in Figure 7 also clearly illustrate the effects of temperature on the high-rate mechanical response of the SMA. Although the environmental temperature was varied only within a rather narrow range, the resultant stress-strain responses show clear temperature dependence. As the environmental temperature decreases from 50° to 0° C, the slopes of both the loading and unloading portions of the stress-strain loops decrease. When the environmental temperature is below room temperature, i.e., 14° C and 0° C, the strain does not return to zero when the specimen is completely unloaded, as indicated by the residual strain in the unloading stress-strain curves at these temperatures. The specimen eventually recovers all strains at room temperature. This phenomenon indicates that, under high-rate deformation, the reverse phase transformation, which needs thermal energy input, may not be as fast as the forward SIM, which is driven by mechanical stress wave loading. Furthermore, when the environmental temperature is close to A_f of the alloy, the drawing of heat from the specimen to assist the reverse transformation may be so much that the temperature in the specimen is actually below A_f during the unloading, which stops the reverse transformation until more heat is drawn from
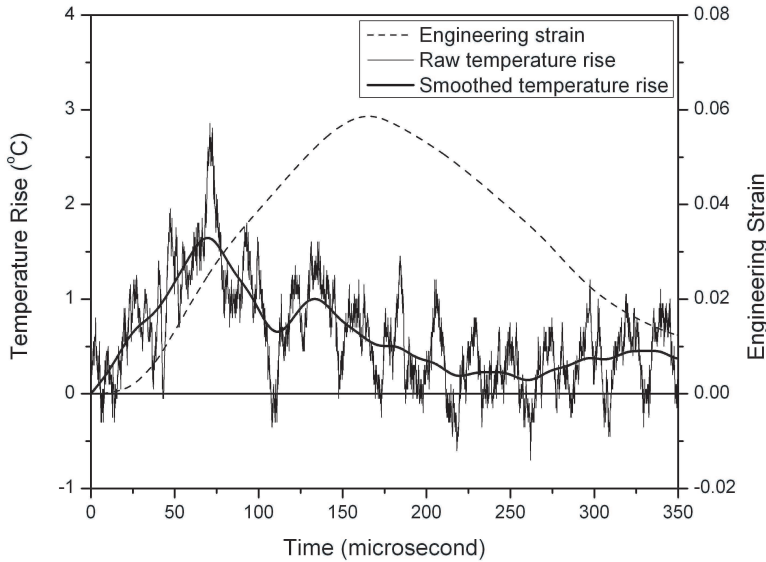
Figure 8. Local temperature variations in the NiTi SMA during
dynamic deformation.

the environment around the specimen to drive the specimen temperature back above
A_f. It is also observed that, although $0°$ C is below A_f of the SMA, superelasticity is still reached. This indicates that the forward SIM driven by stress actually releases heat into the specimen, resulting in the actual specimen temperature above A_f during the superelastic deformation in the specimen. A similar phenomenon was also observed in a previous study, although the testing conditions were not controlled during the unloading stages of the dynamic experiments [Chen et al. 2001].

3.3. *Temperature variation in specimen during dynamic tests.* To better understand the temperature effects on the mechanical response of the NiTi SMA, besides the variations in environmental temperature, the temperature change in the specimen during dynamic deformation needs to be monitored. To accurately monitor the local temperature change during high-rate deformation, a small hole was drilled along the centerline of the cylindrical specimen from one end, and a small thermocouple was placed inside [Song et al. 2003]. The temperature variation during one experiment from the base room temperature is shown in Figure 8. The results in Figure 8 indicate that the specimen temperature rises with increasing strain in the specimen during early stages of loading. The forward SIM driven by mechanical stress waves clearly releases heat as evidenced by the temperature rise. Partly due to the small superelastic strain achieved in the experiments, the amplitude of the temperature rise is rather small. A distinctive and interesting feature

recorded in the temperature history is that the temperature starts to decrease before the maximum strain is reached. In the records shown in Figure 8, the specimen temperature recorded by the small thermocouple starts to decrease at only half of the maximum strain. This repeatable phenomenon in experiments indicates that the deformation in the specimen may not be uniform. With a small hole drilled to accommodate the thermocouple, there are inevitable stress concentrations around the hole, where the SIM driven by the locally concentrated stresses occurs much earlier than the rest of the specimen, resulting in locally higher temperature around the hole. At half of the average maximum strain experienced by the entire specimen, the SIM near the hole is completed. Without further thermal energy released from the SIM, the heat in the specimen actually flows from near the hole to the rest of the specimen, resulting in a decrease in local temperature even though the entire specimen is still under compression. Iadicola and Shaw [2004] showed analytically that SIM occurs at localized transformation fronts even in samples without stress concentrations. The results in Figure 8 also clearly show the existence of specimen temperature changes during dynamic deformation of the SMA. This fluctuation in temperature may drive the specimen material above A_f even though the starting temperature is below A_f. On the other hand, during the reverse transformation, the specimen temperature may drop below A_f to stop the reverse transformation. These results indicate that, depending on the environmental temperature, there is a frequency range where the SMA may be used for dynamic energy dissipation. If the loading/deformation frequency in the application is too high, the transformations— in particular, the reverse transformation in the alloy—may not be fast enough to satisfy the impact/vibration energy dissipation requirements. Furthermore, the temperature variation in the specimen causes a changing temperature behind a specific dynamic stress-strain curve. This nonisothermal testing condition during stress-wave loading causes the shape of the resultant stress-strain curves to deviate from the typical curves obtained under quasistatic loading conditions.

4. Conclusions

A new SHPB technique was employed to determine the dynamic compressive stress-strain behavior of a Nitinol SE508 SMA in its superelasticity phase at a dynamic strain rate of 430/s over an environmental temperature range of 0° to 50° C. The experimental technique had pulse shapers to control both the dynamic loading and unloading profiles to control the loading on the specimen so that the specimen deformed under dynamic stress equilibrium at a constant strain rate during both the loading and unloading stages of the experiments. Local temperature in the specimen was also monitored during dynamic deformation to record the effects of adiabatic heating and cooling associated with the high-rate deformation of the

specimen. Valid dynamic testing conditions were checked for each experiment to ensure that the experiments were valid and the results accurate.

Experimental results show that the compressive stress-strain behavior of the SMA is dependent on both temperature and strain rate. The higher the environmental temperature within the range explored in this study, the stiffer the stress-strain behavior. The shape of the dynamic stress-strain loops obtained over the entire environmental temperature range differs from those obtained quasistatically. Under dynamic loading conditions, the forward and reverse SIM plateaus are inclined, mainly due to temperature variations in the specimen caused by adiabatic heating and cooling during dynamic loading and unloading. The unloading portions of the dynamic compressive stress-strain curves obtained below room temperature exhibit residual strains after the specimen is completely unloaded. This is because the reverse transformation may be stopped when the specimen temperature drops below A_f during unloading.

References

[Belyaev et al. 2002] S. P. Belyaev, N. F. Morozov, A. I. Razov, A. E. Volkov, L. Wang, S. Shi, S. Can, J. Chen, and X. Dong, "Shape-memory effect in titanium-nickel after preliminary dynamic deformation", *Mater. Sci. Forum* **394–395** (2002), 337–340.

[Bhattacharya 2003] K. Bhattacharya, *Microstructure of Martensite: why it forms and how it gives rise to shape memory effort*, Oxford Univ. Press, Oxford, 2003.

[Bhattacharya and James 2005] K. Bhattacharya and R. D. James, "The material is the machine", *Science* **307**:5706 (2005), 53–54.

[Birman 1997] V. Birman, "Review of mechanics of shape memory alloy structures", *Appl. Mech. Rev.* **50**:11 (1997), 629–645.

[Chen et al. 2001] W. W. Chen, Q. Wu, J. H. Kang, and N. A. Winfree, "Compressive superelastic behavior of a NiTi shape memory alloy at strain rates of 0.001-750 s^{-1}", *Int. J. Solids Struct.* **38**:50–51 (2001), 8989–8998.

[Dai et al. 2004] X. Dai, Z. P. Tang, S. Xu, Y. Guo, and W. Wang, "Propagation of macroscopic phase boundaries under impact loading", *Int. J. Impact Eng.* **30**:4 (2004), 385–401.

[Duerig and Pelton 1994] T. W. Duerig and A. R. Pelton, "Ti-Ni shape memory alloys", pp. 1035–1048 in *Materials properties handbook, titanium alloys*, ASM International, Materials Park, Ohio, 1994.

[Duffy et al. 1971] J. Duffy, J. D. Campbell, and R. H. Hawley, "On the use of torsional Hopkinson bar to study rate effects in 1100-0 aluminum", *J. Appl. Mech.* (*ASME*) **38** (1971), 83–91.

[Follansbee 1985] P. S. Follansbee, "The Hopkinson bar", pp. 198–217 in *Mechanical testing, metals handbook*, 9th ed., vol. 8, American Society for Metals, Materials Park, Ohio, 1985.

[Frew et al. 2002] D. J. Frew, M. J. Forrestal, and W. Chen, "Pulse-shaping techniques for testing brittle materials with a split Hopkinson pressure bar", *Exp. Mech.* **42**:1 (2002), 93–106.

[Gray 2000] G. T. Gray, III, "Classic split-Hopkinson pressure bar testing", pp. 462–476 in *ASM handbook: Mechanical testing and evaluation*, vol. 8, edited by H. Kuhn and D. Medlin, ASM International, Materials Park, Ohio, 2000.

[Gray et al. 1997] G. T. Gray, III, W. R. Blumenthal, C. P. Trujillo, and R. W. Carpenter, II, "In-fluence of temperature and strain rate on the mechanical behavior of Adiprene L-100", *J. Phys. (France) IV* **7**:C3 (1997), 523–528. International Conference on Mechanical and Physical Behaviour of Materials under Dynamic Loading (EURODYMAT'97), Toledo (Spain), 22-26 Sep 1997.

[Iadicola and Shaw 2004] M. A. Iadicola and J. A. Shaw, "Rate and thermal sensitivities of unstable transformation behavior in a shape memory alloy", *Int. J. Plast.* **20**:4–5 (2004), 577–605.

[James and Hane 2000] R. D. James and K. F. Hane, "Martensitic transformations and shape-memory materials", *Acta Mater.* **48**:1 (2000), 197–222.

[Kolsky 1949] H. Kolsky, "An investigation of mechanical properties of materials at very high rates of loading", *P. Phys. Soc. Lond. B* **62**:11 (1949), 676–700.

[Lagoudas et al. 2003] D. C. Lagoudas, K. Ravi-Chandar, K. and. Sarh, and P. Popov, "Dynamic loading of polycrystalline shape memory alloy rods", *Mech. Mater.* **35**:10.1016/S0167-6636(02)00199-0 (2003), 689–716.

[Lin et al. 1996] P. H. Lin, H. Tobushi, K. Tanaka, T. Hattori, and A. Ikai, "Influence of strain rate on deformation properties of TiNi shape memory alloy", *JSME Int. J. A Mech. M.* **39**:1 (1996), 117–123.

[Lindholm 1964] U. S. Lindholm, "Some experiments with the split Hopkinson pressure bar", *J. Mech. Phys. Solids* **12**:5 (1964), 317–335.

[Liu et al. 2002] Y. Liu, Y. Li, and K. T. Ramesh, "Rate dependence of deformation mechanisms in a shape memory alloy", *Philos. Mag. A* **82**:12 (2002), 2461–2473.

[Lovey et al. 2004] F. C. Lovey, A. M. Condó, and V. Torra, "A model for the interaction of marten-sitic transformation with dislocations in shape memory alloys", *Int. J. Plast.* **20**:2 (2004), 309–321.

[McNaney et al. 2003] J. M. McNaney, V. Imbeni, Y. Jung, P. Papadopoulos, and R. O. Ritchie, "An experimental study of the superelastic effort in a shape-memory nitinol alloy under biaxial loading", *Mech. Mater.* **35**:10 (2003), 969–986.

[Meyers 1994] M. A. Meyers, *Dynamic behavior of materials*, Wiley-Interscience, New York, 1994. 305–310.

[Millett et al. 2002] J. C. F. Millett, N. K. Bourne, and G. T. Gray, "Behavior of the shape memory alloy NiTi during one-dimensional shock loading", *J. Appl. Phys.* **92**:6 (2002), 3107–3110.

[Nakayama et al. 2005] H. Nakayama, Y. Zhao, M. Taya, W. W. Chen, Y. Urushiyama, and S. Suzuki, "Strain rate effects of TiNi and TiNiCu shape memory alloys", pp. 355–363 in *Proceedings of SPIE, Smart structures and materials 2005: Active materials: Behaviors and mechanics*, vol. 5761, edited by W. D. Armstrong, San Diego, CA, 2005.

[Nemat-Nasser et al. 2005] S. Nemat-Nasser, J. Y. Choi, W. G. Guo, J. B. Isaacs, and M. Taya, "High strain-rate, small strain response of a NiTi shape-memory alloy", *J. Eng. Mater. Technol.* (*ASME*) **127**:1 (2005), 83–89.

[Ogawa 1988] K. Ogawa, "Characteristics of shape memory alloy at high strain rate", *J. Phys.* **49**:C3 (1988), 115–120.

[Otsuka and Wayman 1988] K. Otsuka and C. M. Wayman, *Shape memory materials*, Cambridge Univ. Press, 1988.

[Ravichandran and Chen 1991] G. Ravichandran and W. Chen, "Dynamic behavior of brittle materi-als under uniaxial compression", pp. 85–90 in *Experiments in micromechanics of fracture resistant materials*, edited by K. S. Kim, AMD-130, ASME, New York, 1991.

[Schetky and Perkins 1978] L. M. Schetky and J. Perkins, "The 'quiet' alloys", *Machine Design* **50**:8 (April 6 1978), 202–206.

[Song and Chen 2004] B. Song and W. Chen, "Loading and unloading SHPB pulse shaping techniques for dynamic hysteretic loops", *Exp. Mech.* **44**:6 (2004), 622–627.

[Song et al. 2003] B. Song, W. Chen, and T. Weerasooriya, "Quasi-static and dynamic compressive behaviors of a S-2 glass/SC15 composite", *J. Compos. Mater.* **37**:19 (2003), 1723–1743.

[Song et al. 2005] B. Song, W. Chen, T. Yanagita, and D. J. Frew, "Temperature effects on the dynamic compressive and failure behaviors of an epoxy syntactic foam", *Compos. Struct.* **67**:3 (2005), 289–298.

[Stoeckel and Yu 1991] D. Stoeckel and W. Yu, "Superelastic Ni-Ti wire", *Wire J. Inter.* **24**:3 (March 1991), 45–50.

[Togami et al. 1996] T. C. Togami, W. E. Baker, and M. J. Forrestal, "A split Hopkinson bar technique to evaluate the performance of accelerometers", *J. Appl. Mech.* (*ASME*)) **63** (1996), 353–356.

[Wayman 1993] C. M. Wayman, "Shape memory alloys", MRS Bulletin, April 1993. 49–56.

[Wu and Gorham 1997] X. J. Wu and D. A. Gorham, "Stress equilibrium in the split Hopkinson pressure bar test", *J. Phys. (France) IV* **7**:C3 (1997), 91–96. International Conference on Mechanical and Physical Behaviour of Materials under Dynamic Loading (EURODYMAT'97), Toledo (Spain), 22-26 Sep 1997.

WEINONG CHEN: wchen@purdue.edu
Schools of Aeronautics and Astronautics and Materials Engineering, Purdue University,
West Lafayette, IN 47907-2023, United States

BO SONG: songb@purdue.edu
School of Aeronautics and Astronautics, Purdue University, West Lafayette, IN 47907-2023,
United States